

Two-dimensional Rayleigh-Bénard convection in a closed box with free-slip walls

Ambrish Pandey and Jörg Schumacher
Technische Universität Ilmenau, Germany

1 Introduction

We study Rayleigh-Bénard convection (RBC) in a two-dimensional closed box of aspect ratio four (aspect ratio = length/height). RBC is an idealized model of thermal convection in which a fluid layer placed between two horizontal plates is heated from below and cooled from above [1, 3, 2]. Two important quantities in RBC are the Nusselt number and the Reynolds number. The Nusselt number (Nu) is a nondimensional measure of the turbulent heat transport, whereas the Reynolds number is a nondimensional measure of the turbulent momentum transport.

2 Governing Equations

Conservation of mass, momentum, and internal energy lead to equations which govern the dynamics of RBC. In the Boussinesq approximation [2] they are given by

$$\frac{\partial \mathbf{u}}{\partial t} + \mathbf{u} \cdot \nabla \mathbf{u} = -\frac{\nabla p'}{\rho_0} + \alpha g (T - T_0) \hat{z} + \nu \nabla^2 \mathbf{u}, \quad (1)$$

$$\frac{\partial T}{\partial t} + \mathbf{u} \cdot \nabla T = \kappa \nabla^2 T, \quad (2)$$

$$\nabla \cdot \mathbf{u} = 0, \quad (3)$$

where $\mathbf{u} = (u_x, u_y, u_z)$, T , and p' are the velocity, temperature, and pressure fluctuation fields, respectively. Quantities α, ν, κ are thermal expansion coefficient, kinematic viscosity, and thermal diffusivity of the fluid, respectively. Quantities ρ_0 and T_0 denote reference values of mass density and temperature. The acceleration due to gravity g is pointed in the downward, in $-\hat{z}$ direction.

The aforementioned equations still carry physical dimensions. However it is convenient to study nondimensional equations. To nondimensionalize the above equations, we use the following transformation:

$$\mathbf{x} \rightarrow \tilde{\mathbf{x}} = \frac{\mathbf{x}}{H} \quad (4)$$

$$\mathbf{u} \rightarrow \tilde{\mathbf{u}} = \frac{\mathbf{u}}{u_f} \quad (5)$$

$$t \rightarrow \tilde{t} = \frac{tu_f}{H} \quad (6)$$

$$T \rightarrow \tilde{T} = \frac{T}{\Delta T}, \quad (7)$$

$$p \rightarrow \tilde{p} = \frac{p}{\rho_0 u_f^2}. \quad (8)$$

Here H is the distance between two horizontal plates or the height of the box and $\Delta T (= T_{\text{bottom}} - T_{\text{top}} > 0)$ is the temperature difference between them. Time is measured in units of the free-fall time $t_f = H/u_f$, and velocities are given in units of the free-fall velocity, $u_f = \sqrt{\alpha g \Delta T H}$. The nondimensional RBC equations are

$$\frac{\partial \tilde{\mathbf{u}}}{\partial \tilde{t}} + \tilde{\mathbf{u}} \cdot \tilde{\nabla} \tilde{\mathbf{u}} = -\tilde{\nabla} p + \tilde{T} \hat{z} + \sqrt{\frac{Pr}{Ra}} \tilde{\nabla}^2 \tilde{\mathbf{u}}, \quad (9)$$

$$\frac{\partial \tilde{T}}{\partial \tilde{t}} + \tilde{\mathbf{u}} \cdot \tilde{\nabla} \tilde{T} = \frac{1}{\sqrt{Pr Ra}} \tilde{\nabla}^2 \tilde{T}, \quad (10)$$

$$\tilde{\nabla} \cdot \tilde{\mathbf{u}} = 0. \quad (11)$$

Two nondimensional parameters appear in above equations, which are the main governing parameters of RBC. The Rayleigh number (Ra) is the measure of the thermal driving force, and the Prandtl number (Pr) is a ratio of the kinematic viscosity and thermal diffusivity of the fluid. They are defined as

$$Ra = \frac{\alpha g \Delta T H^3}{\nu \kappa}, \quad (12)$$

$$Pr = \frac{\nu}{\kappa}. \quad (13)$$

For relatively small temperature gradients, heat transport occurs via conduction only, and temperature varies linearly from the bottom to the top, satisfying

$$T_{\text{cond}}(z) = T_{\text{bottom}} - \frac{\Delta T}{H} z, \quad (14)$$

where T_{bottom} is the temperature at the bottom plate. However, the temperature starts fluctuating in space and time once the convection has established in the system. It is customary to separate temperature fluctuations θ from the mean conduction profile, and analyze the equation for θ , where

$$\theta(x, y, z) = T(x, y, z) - T_{\text{cond}}(z). \quad (15)$$

The nondimensional RBC equations in terms of θ are

$$\frac{\partial \tilde{\mathbf{u}}}{\partial \tilde{t}} + \tilde{\mathbf{u}} \cdot \tilde{\nabla} \tilde{\mathbf{u}} = -\tilde{\nabla} p + \tilde{\theta} \hat{z} + \sqrt{\frac{Pr}{Ra}} \tilde{\nabla}^2 \tilde{\mathbf{u}}, \quad (16)$$

$$\frac{\partial \tilde{\theta}}{\partial \tilde{t}} + \tilde{\mathbf{u}} \cdot \tilde{\nabla} \tilde{\theta} = \tilde{u}_z + \frac{1}{\sqrt{Pr Ra}} \tilde{\nabla}^2 \tilde{\theta}, \quad (17)$$

$$\tilde{\nabla} \cdot \tilde{\mathbf{u}} = 0, \quad (18)$$

where $\tilde{\theta} = \theta/\Delta T$. From now on we drop the tilde.

3 Boundary Conditions

In direct numerical simulations (DNS), we need to specify boundary conditions to solve the RBC equations. In case of the no-slip boundary condition, which occurs at a rigid wall, all the components of velocity vanish at the specified boundary, i.e., $\mathbf{u} = \mathbf{0}$. For a stress-free condition the fluid can slip along the wall, but cannot penetrate. At a stress-free boundary, the normal component of velocity as well as the normal derivative of the tangential components of velocity, vanish, i.e., $u_n = 0; \partial u_t / \partial n = 0$. For the temperature field, usually the conducting

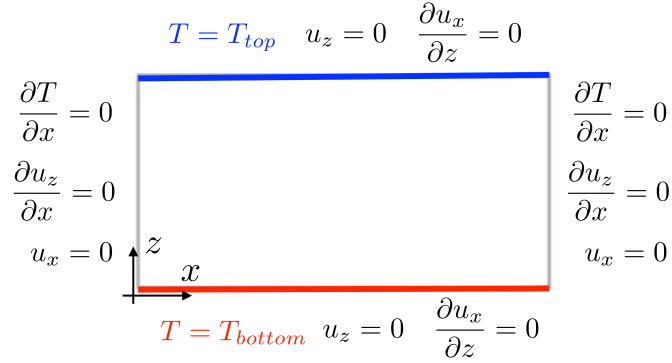


Figure 1: Schematic of boundary conditions in the present 2D DNS.

boundary condition is applied at the top and bottom plates, where the temperature is fixed, i.e., $T = \text{constant}$. At the sidewalls, adiabatic or perfectly thermally insulated condition is usually employed, where the normal derivative vanishes, i.e., $\partial T/\partial n = 0$. The boundary conditions for the present case are summarized in Fig. 1.

4 Numerical Method

We assume that all the fields $u_x, u_z, T \in L^2(\Omega)$, with $\Omega = [0, L_x] \times [0, H]$. Equations (16–18) are solved using a pseudospectral solver TARANG [5] in a two-dimensional box of aspect ratio $\Gamma = L_x/H = 4$. Stress-free boundary condition for the velocity field is employed at all the walls. For the temperature field, isothermal (adiabatic) boundary condition is employed in the vertical (horizontal) direction. To satisfy these boundary conditions, the temperature fluctuation and velocity components are expanded in sine and cosine basis functions, which are

$$u_x(x, z) = \sum_{k_x, k_z} 4\hat{u}_x(k_x, k_z) \sin(k_x x) \cos(k_z z), \quad (19)$$

$$u_z(x, z) = \sum_{k_x, k_z} 4\hat{u}_z(k_x, k_z) \cos(k_x x) \sin(k_z z), \quad (20)$$

$$\theta(x, z) = \sum_{k_x, k_z} 4\hat{\theta}(k_x, k_z) \sin(k_x x) \cos(k_z z), \quad (21)$$

where $\mathbf{k} = (k_x, k_z)$ is the wavevector [4] with $k_x = m\pi/L_x$ and $k_z = n\pi/H$; m, n being integers. We perform direct numerical simulation for $\text{Pr} = 10, \text{Ra} = 10^6$, and $\Gamma = 4$ using 513×129 uniformly spaced grid points. The time advancement is done using fourth order Runge-Kutta method (RK4), and fields are dealiased using 2/3 rule. We refer to Verma *et al.* [4, 5] for more details of the numerical simulations.

5 Results

We start our simulation using random temperature and velocity fields, and continue until the statistically stationary state is reached. Total duration of the simulation is $5000 t_f$. In Fig. 2, the Nusselt number is shown as a function of time. The Nusselt number is the ratio of the total

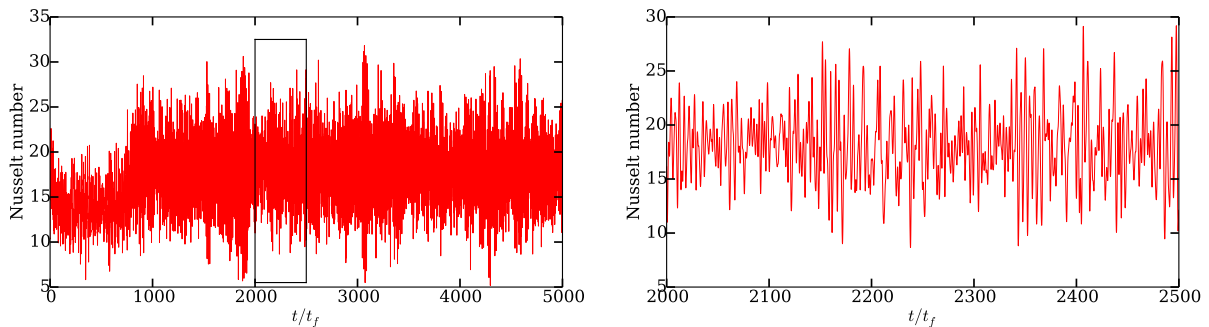


Figure 2: Time series of the Nusselt number. A zoom over the rectangular box is shown in right panel. In this range, 5001 snapshots of the velocity and temperature field have been generated, which are separated by 0.1 time units.

heat transport to the conductive heat transport, which is computed at each horizontal line as

$$Nu(z) = \frac{\langle u_z T \rangle_{x,t} - \kappa \frac{\partial \langle T \rangle_{x,t}}{\partial z}}{\kappa \frac{\Delta T}{H}} = \text{const.} \quad (22)$$

For pure heat conduction $Nu = 1$ by definition. Equation (22) is a consequence of line-temporal averaging of Eq. (2). Here $\langle \rangle_{x,t}$ represents the averaging over a horizontal line x at a given z , as well as over time. If we perform the vertical averaging of the above equation, we get

$$Nu = 1 + \frac{H}{\kappa \Delta T} \langle u_z T \rangle_{A,t}, \quad (23)$$

where $\langle \rangle_A$ represent the area-averaging over the entire 2D box.

Reynolds number is a measure of the strength of the nonlinear term compared to the viscous term in the momentum equation [Eq. (1)], which is computed as

$$Re = UH/\nu, \quad (24)$$

where U is the root mean square velocity, which is given by

$$U = \sqrt{\langle u_x^2 \rangle_{A,t} + \langle u_z^2 \rangle_{A,t}}. \quad (25)$$

In our DNS we compute U from the kinetic energy per unit mass $E_u(x, z, t) = \mathbf{u}^2/2$ as

$$U = \sqrt{2 \langle E_u \rangle_{A,t}}. \quad (26)$$

The kinetic energy is alternatively computed using the sum over all the Fourier modes

$$E_u(t) = \frac{1}{2A} \int_A \mathbf{u}^2 dA = \sum_{\mathbf{k}} \frac{1}{2} |\hat{u}(\mathbf{k})|^2. \quad (27)$$

We plot the time series of kinetic energy in Fig. 3.

Figure 4 shows the instantaneous temperature and velocity fields at two different times. The top panel (at $t = 500 t_f$) shows that one-roll structure is dominant, whereas the bottom panel (at $t = 2250 t_f$) shows a dominant two-roll structure. It is also clear from Figs. 2 and 3, that a change in the convective pattern has occurred at around $t = 1000 t_f$. Beyond $t \approx 1000 t_f$, the convection

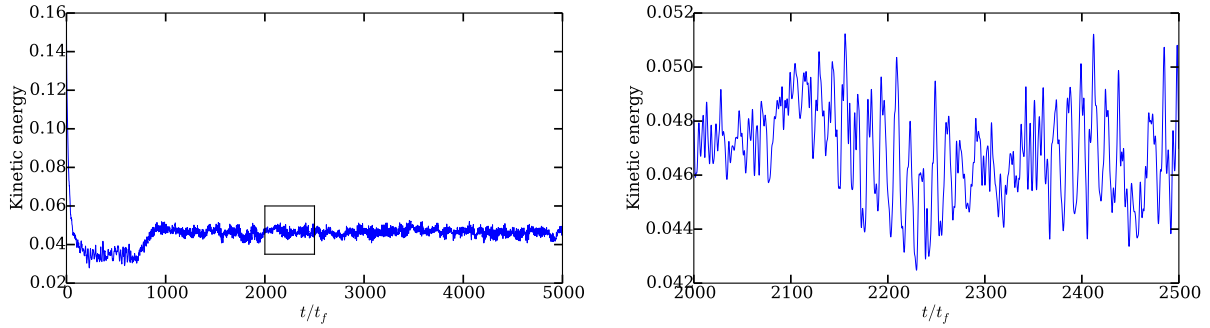


Figure 3: Kinetic energy $E_u(t)$ as a function of time. Right panel shows again the zoom of portion inside the rectangular box.

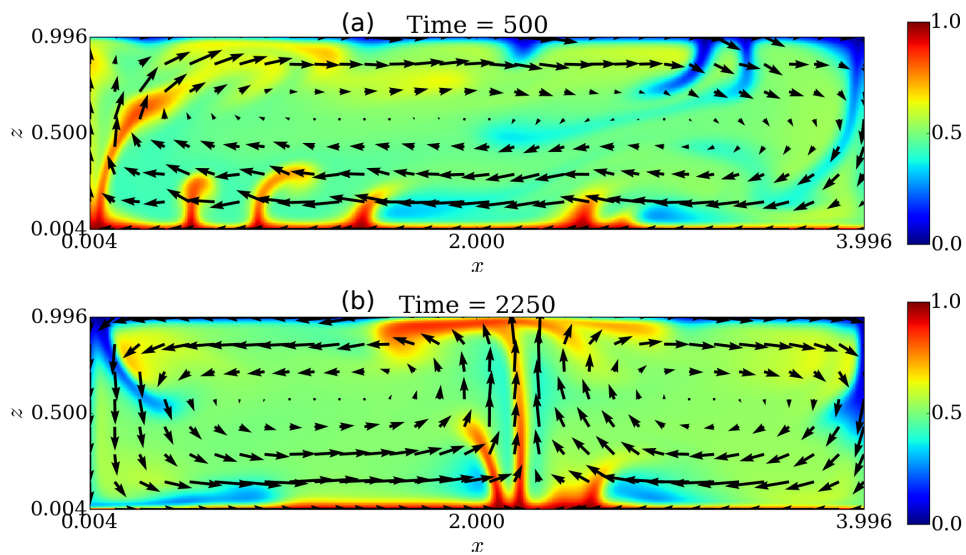


Figure 4: Temperature and velocity field at $t = 500 t_f$ (top panel) and at $t = 2250 t_f$ (bottom panel). Temperature field is shown using a color scale with red (blue) structures representing hot fluid going upward (downward). The corresponding velocity field is represented using arrows.

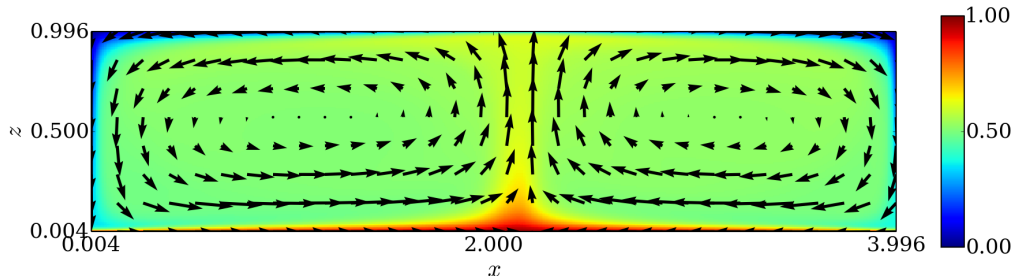


Figure 5: [NEW] Time-averaged temperature and velocity fields. Turbulent fluctuations have been removed by time-averaging, therefore the fields look smooth when compared to an instantaneous snapshot [Fig. 4(b)].

Table 1: Some details about the simulation. L_x and H are the length and height of the box, N_x and N_z and the number of grid intervals in x - and z -direction respectively, t_η and η_K are the mean Kolmogorov time and Kolmogorov length in the statistically steady state, and l_{\min} is the mesh width of the uniform grid.

Pr	Ra	L_x	H	N_x	N_z	Nu	Re	t_η	η_K	l_{\min}
10	10^6	4	1	512	128	17.7	95.5	0.77	0.0495	0.0078

pattern is dominated by two-roll structure till the final simulation time ($t = 5000 t_f$), which oscillates a bit back and forth. Table 1 summarizes some details of our simulation parameters.

[NEW] Figure 5 shows the mean temperature and velocity fields averaged for $500 t_f$ between $t = 2000 t_f$ and $t = 2500 t_f$. The figure exhibits a clear two-roll structure with hot fluid rising from the center and cold fluid descending at the sidewalls. In addition, the bulk temperature T_m follows to

$$T_m = \langle T \rangle_{A,t} = \frac{1}{2}. \quad (28)$$

[NEW] The Nusselt number at a given height is computed as $Nu(z) = \sqrt{RaPr} \langle u_z T \rangle_{x,t} - \frac{\partial \langle T \rangle_{x,t}}{\partial z}$, where u_z, T are nondimensional variables. We plot the horizontal profile of the convective heat flux $\sqrt{RaPr} u_z (T - T_m)$ at $z = \delta_T$ and $z = H/2$ in Fig. 6. For an instantaneous snapshot (shown in Fig. 4(b) for $t = 2250 t_f$), convective flux highly fluctuates at the mid-height. It shows strong positive peaks near the center and sidewalls, where the fluid is ascending and descending respectively [see Fig. 4(b)]. At $z = \delta_T$, however, the variations of profile are less pronounced, which is due to the dominance of horizontal velocity near the top and bottom plates. We observe a qualitatively similar behavior for the time-averaged convective flux. In this case profiles appear to be more symmetric about the center. Figure 7 shows the horizontal profile of conductive heat flux $\frac{\partial T}{\partial z}$ at $z = H/2$. The profile of the time-averaged field is smoother. It is also apparent that near the center and the sidewalls magnitude of the convective flux is much larger (approximately two orders in magnitude) compared to that of the conductive flux.

6 Details about the data structure

Velocity and temperature fields are written in hdf5 file format. Fields at time t_f can be found in ‘real. t_f ’ folder, where $t_f = 2000, 2000.1, 2000.2, \dots, 2499.9, 2500$. Three files are there is each

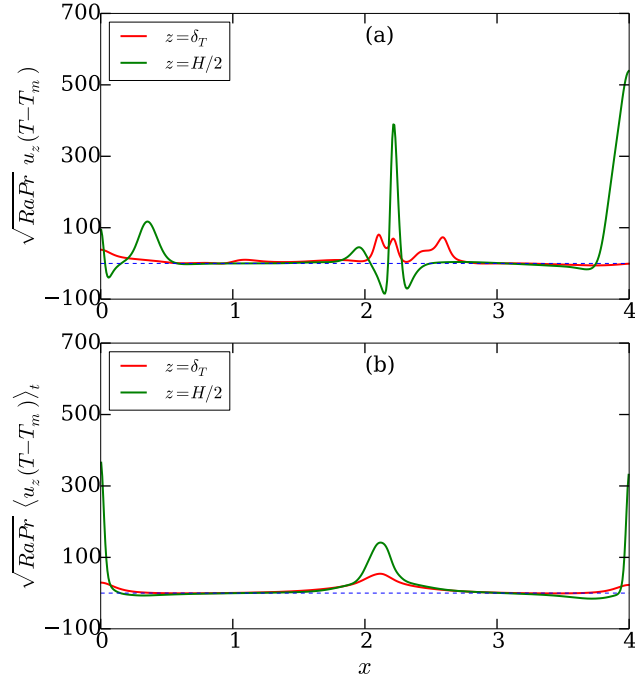


Figure 6: [NEW] Horizontal profile of the convective heat flux for an instantaneous snapshot at $t = 2250 t_f$ [panel (a)] and for the time-averaged fields [panel (b)]. At the mid-height, strong peaks are observed near the center and the sidewalls, whereas at the thermal boundary layer height, convective flux is smoother. Time-averaged profiles are almost symmetric about the center, and show smaller peaks near the center and the sidewalls.

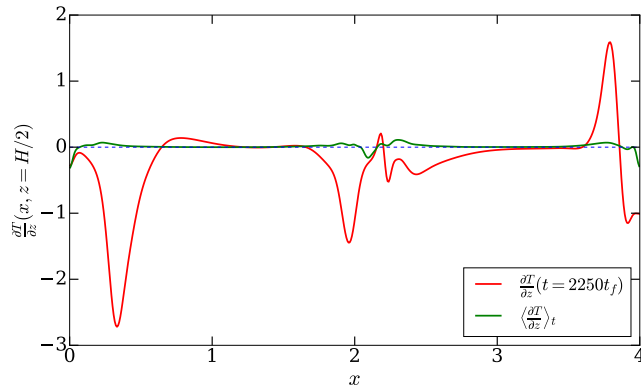


Figure 7: [NEW] Horizontal profile of the conductive heat flux $\frac{\partial T}{\partial z}$ at the mid-height for a snapshot (red curve) and for the time-averaged field (green curve).

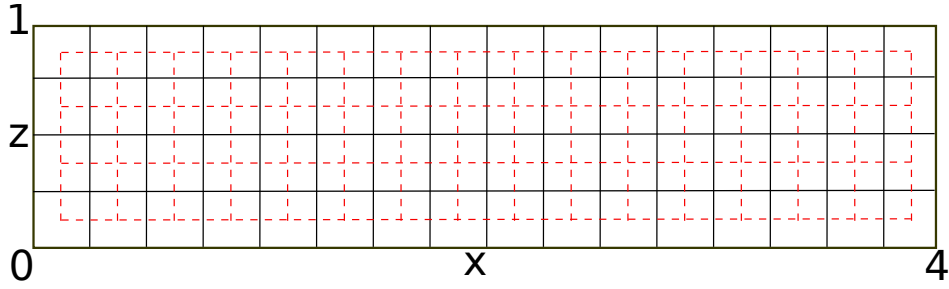


Figure 8: A schematic of the discretization of the simulation domain. The grid shown as solid black lines represents how the box is discretized for simulation. However, the field values are stored at the center of each cell, i.e., at the crossings of the grid exhibited as the dashed red lines.

folder, two for velocity components u_x, u_z and one for temperature fluctuation.

File `T.Fr.h5` contains the temperature fluctuation field at 512×128 grid points. Similarly, file `U.V1r.h5` contains the z-component of the velocity field (u_z), and file `U.V3r.h5` contains the x-component of the velocity field (u_x). **Kindly note that the file `U.V3r.h5` contains the u_x , not the u_z field.**

6.1 Coordinates of the velocity and temperature fields

For simulation, the box is uniformly divided into 512 grid intervals in x-direction and 128 grid intervals in z-direction, which yield

$$\begin{aligned} dx &= L_x/N_x = 4/512 = 0.0078125, \\ dz &= H/N_z = 1/128 = 0.0078125. \end{aligned}$$

Computations are carried out in Fourier space. However to get the velocity and temperature field in real space the FFTW library is used, which omit the values at the boundary. Therefore in x-direction, the real fields are stored from $dx/2$ to $L_x - dx/2$ at the interval of dx . Similarly, in z-direction, the fields are stored from $dz/2$ to $H - dz/2$ at the interval of dz . The u_x, u_z , and θ fields are stored at 512×128 inner points (shown in Fig. 8) whose x-coordinates are

$$x = [0.00390625, 0.01171875, 0.01953125, \dots, 3.98046875, 3.98828125, 3.99609375],$$

and z-coordinates are

$$z = [0.00390625, 0.01171875, 0.01953125, \dots, 0.98046875, 0.98828125, 0.99609375].$$

7 Post-processing of data

The hdf5 files can be post processed for visualization using matlab and matplotlib softwares.

7.1 Using ‘matplotlib’

We need to import ‘h5py’ library to work with hdf5 files. To read the file do the following:

```
file_t = h5py.File('T.Fr.h5', 'r')
```

```

dset_t = file_t['/T.Fr']
theta = dset_t[:,:]
file_ux = h5py.File('U.V3r.h5', 'r')
dset_ux = file_ux['/U.V3r']
ux = dset_ux[:,:]
file_uz = h5py.File('U.V1r.h5', 'r')
dset_uz = file_uz['/U.V1r']
uz = dset_uz[:,:]

```

Thus we have stored the velocity and temperature fluctuation fields as 2D arrays in variables `ux`, `uz` and `theta`. Now one can do further array operations using these variables. **Please note that the file 'T.Fr.h5' contains the temperature fluctuation field $\theta(x, z)$, not the temperature field $T(x, z)$. We need to construct the temperature field using $T(x, z) = 1 - z + \theta(x, z)$, since the nondimensional temperature at the bottom $T_b = 1$, and also $\Delta T = 1, H = 1$.**

7.2 Using 'matlab'

Files can be read in matlab using the following commands:

```

theta = hdf5read('T.Fr.h5', '/T.Fr');
ux = hdf5read('U.V3r.h5', '/U.V3r');
uz = hdf5read('U.V1r.h5', '/U.V1r');

```

Then further processing can be done using the above 2D arrays.

8 Derivatives of the velocity and temperature fluctuation fields

[NEW]

We have computed all the spatial derivatives of the instantaneous fields u_x, u_z, θ using spectral method, and put them in folders named 'real $_t$ '. These folders are placed within a folder named 'derivatives'. Each folder named 'real $_t$ ' contains six files named `dTdx.Fr.h5`, `dTdz.Fr.h5`, `dudx.Fr.h5`, `dudz.Fr.h5`, `dwdx.Fr.h5`, `dwdz.Fr.h5`, which contain the derivatives $\partial\theta/\partial x$, $\partial\theta/\partial z$, $\partial u_x/\partial x$, $\partial u_x/\partial z$, $\partial u_z/\partial x$, $\partial u_z/\partial z$, respectively. These derivatives are stored at the same grid points where the fields are stored (see Sec. 6.1). **Please note that the files `dTdx.Fr.h5`, `dTdz.Fr.h5` contain the derivatives of temperature fluctuation field θ and not of the temperature field $T(= 1 - z + \theta)$.** We can read these files as

```

file_t = h5py.File('dTdx.Fr.h5', 'r')
dset_t = file_t['/dTdx.Fr']
dTdx = dset_t[:,:]

```

Other files can be loaded and post processed similarly.

References

- [1] AHLERS, G., GROSSMANN, S., AND LOHSE, D. Heat transfer and large scale dynamics in turbulent Rayleigh-Bénard convection. *Rev. Mod. Phys.* 81 (2009), 503–537.
- [2] CHILLÀ, F., AND SCHUMACHER, J. New perspectives in turbulent Rayleigh-Bénard convection. *Eur. Phys. J. E* 35 (2012), 58.
- [3] LOHSE, D., AND XIA, K. Q. Small-scale properties of turbulent Rayleigh-Bénard convection. *Annu. Rev. Fluid Mech.* 42 (2010), 335–364.

- [4] VERMA, M. K., AMBHIRE, S. C., AND PANDEY, A. Flow reversals in turbulent convection with free-slip walls. *Phys. Fluids* 27 (2015), 047102.
- [5] VERMA, M. K., CHATTERJEE, A. G., REDDY, K. S., YADAV, R. K., PAUL, S., CHANDRA, M., AND SAMTANEY, R. Benchmarking and scaling studies of a pseudospectral code tarang for turbulence simulations. *Pramana* 81, 4 (2013), 617–629.